Engineering Journal issn: 0125-8281

Article

In-situ Observation of h-BN Formation on the Surface of Weld Dissimilar Joint Steels

Chanan Euaruksakul[1,a], Isaratat Phung-on[2,b,*], Jongkol Srithorn[3,c], Thipusa Wongpinij[1,d], Pat Photongkam[1,e], Krongthong Kamonsuangkasem[1,f], and Neeranut Aimkogsung[1,g]

1 Synchrotron Light Research Institute (Public Organization), Nakhon Ratchasima 30000, Thailand
2 Institute for Scientific and Technological Research and Services, King Mongkut's University of Technology Thonburi, Bangkok 10140, Thailand
3 Industrial Engineering Institute of Engineering, Suranaree University of Technology, Nakhon Ratchasima 30000, Thailand
E-mail: [a]chanan@slri.or.th, [b,*]isaratat.phu@kmutt.ac.th (Corresponding author), [c]jongkol@sut.ac.th, [d]thipusa@slri.or.th, [e]pat@slri.or.th, [f]krongthong@slri.or.th, [g]neeranut2531@gmail.com

Abstract. In-situ observation of h-BN formation by surface precipitation on the surface of joined dissimilar steels is presented. Because the substrate consists of two different types of steels, different growth behaviors can be seen on different sides and also in the middle of the weld interface. This observation demonstrates that formations of 2D materials can occur on surfaces of steels under suitable conditions e.g. temperature, microstructures and concentrations of impurities. Characterizations by electron microscopy and synchrotron spectroscopy technics confirm that h-BN crystals that appear on the surface after annealing are of similar quality to those prepared by other methods such as chemical vapor deposition. Moreover, real-time observation during sample temperature swing above and below the phase transition temperature of Fe shows that h-BN islands reversibly form and dissociate on the surface. The results show that the formation of h-BN on steels is reversible and the analysis suggests that the process is likely affected by structural change of the steels near the phase transition temperature, which in-turn drives the diffusions of B and N atoms back and forth between surface and bulk.

Keywords: h-BN, surface precipitation, low-energy electron microscopy, photoemission electron microscopy, welded metals.

ENGINEERING JOURNAL Volume 25 Issue 5
Received 29 September 2020
Accepted 1 May 2021
Published 31 May 2021
Online at https://engj.org/
DOI:10.4186/ej.2021.25.5.81

DOI:10.4186/ej.2021.25.5.81

1. Introduction

Two-dimensional materials have attracted interest in material research communities due to the newly discovered properties which come from the thickness of just one or few atomic layers. The extremely small thickness triggers quantum size effect which strongly modifies the electronic structures and the carrier transports of these materials, in many cases resulting in new unique properties suitable for a wide range of applications [1]-[5]. The thickness measured in angstroms which is extremely small in comparison to the lateral size makes them able to withstand sharp bending while retaining perfect crystalline structures. This makes most two-dimensional materials suitable for applications that required mechanical flexibility such as for flexible electronic devices [6]-[8] in which h-BN is a unique choice to be used as an electrically insulating layer due to its relatively wide (direct) bandgap of around 5.9 eV [9]. h-BN can also be potentially used for surface modifications, such as for corrosion prevention [10], for being a nano-reactor for confined catalysis [11], and for friction reduction in lubrication engineering [12]. While fabrication of few-layer h-BN is conventionally performed by chemical vapor deposition (CVD) process in which borazine is deposited on a catalytic surface such as Rh(111) and then decomposed into h-BN layers by heat [13, 14], or by exfoliation from a bulk crystal that is suitable for stacking h-BN on other types of 2D materials [15, 16], h-BN also forms on surface of some metals or alloys at high temperature if there are small amounts of B and N impurities inside the bulk. B and N diffuse and segregate on the surface to form crystalline h-BN precipitations. One approach that has recently been developed and shows promising results for metallurgical applications is to deposit BN film by magnetron sputtering on one side of a thin Ni, Fe or Co foils or layers, and then anneal the samples to drive B and N to the un-deposited side to form few-layer h-BN [17-19]. In the prospect of surface modification of alloys that are used as engineering materials, h-BN has a tendency to perform as a protective layer, providing inert, low-friction and low-degassing surface to make the modified metals work more effectively, for examples, under harsh environmental conditions. We chose to study formation of h-BN on welding joint between dissimilar steels as it is expected that h-BN layer that form may help to reduce the effect of carbon diffusion and creep failure when the materials are used under high temperature and pressure where carbon deposit may occur on the surface due to contact to the flow of gases or liquids containing carbonaceous molecules.

With aforementioned methods to create h-BN layers on surface of metals, there remains the difficulty to control the coverages, thicknesses and crystallographic orientations of the h-BN [3]. In this work, we present an observation of h-BN formation by the surface precipitation method near the interface region of two joined steels, each containing different alloy compositions, to investigate the mechanism that creates h-BN. By using low-energy electron microscopy (LEEM), we record the growth of h-BN on the surface at the joined interface in real-time. The effect of composition gradient on the diffusion of B and N atoms both vertically between surface and bulk, and laterally along the interface between the two alloys are investigated to find major factors that affect reaction mechanism for h-BN formation by the precipitation method in this complex alloy system. Photoemission electron microscopy (PEEM) with synchrotron radiation was also used to identify chemical states of h-BN created in the experiment.

2. Materials and Methods

2.1. Sample Descriptions

The samples used in this study consist of 2.25Cr-1Mo Steel which was overlay welded by ER90S-B9 filler metal and was originally made for a study of welding process that focused on C migration [20, 21]. The sample was prepared by joining the two dissimilar metal alloys together by welding (the schematic diagram of the sample is shown in Fig. 1 and the composition table describing the atomic concentration of each alloy is given in Table 1. In the welding process, the base metal (A) is a Fe alloy with lower Cr contents (2.25Cr-1Mo) and the weld metal on the other side (B) is a high-Cr (stainless steel - ER90S-B9). Metal B was bead-on-plate welded on Metal A. The joined steel was cut, thinned and then polished to expose the cross-section near the interface. The final thickness of the sample was around 200 μm. Three regions from the welding process were exposed for LEEM observation: the heat-affected zone on the Metal A side, the weld zone where metal B melted and then solidify (creating epitaxial growth of Fe) during the welding process, and the interfacial zone in between. The sample was mounted on a sample cartridge of the LEEM/PEEM system which was capable of heating up by using electron bombardment from the backside.

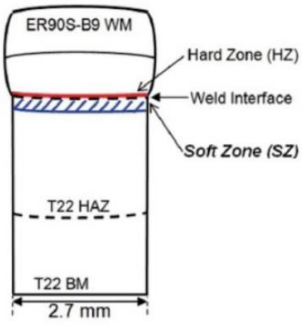

Fig. 1. Schematic diagram of the sample in this work.

The small amount of B was detected inside the sample as detected by wavelength-dispersive x-ray fluorescence (XRF) (Fig. 2). N mapping was not shown due to the detection limit of the XRF measurement setup. After the

welding, the sample was cut to expose the cross-section containing the Metal A (2.25Cr-1Mo), Metal B (ER90S-B9 filler metal) and the weld interface. The cross-sectioned sample was then thinned and polished to the mirror-like finish so that under LEEM, the work function contrast was clear. With LEEM, the different grain structures of the weld metal and the heat-affected zone of the base metal could be easily distinguished. The base metal side of the sample was also confirmed with a marker made by a hardness indentation.

Table 1. Composition table of 2.25C4-1Mo (Metal A) and ER90S-B9 (Metal B).

Type of material	Chemical composition (wt-%)					
	C	Mn	Si	Ni	Cr	Mo
2.25Cr-1Mo (Metal A)	0.05-0.15	0.30-0.60	0.50	0.25	1.90-2.60	0.87-1.13
ER90S-B9 (Metal B)	0.08-0.12	1.20	0.20-0.50	0.80	8.00-9.50	0.85-1.05

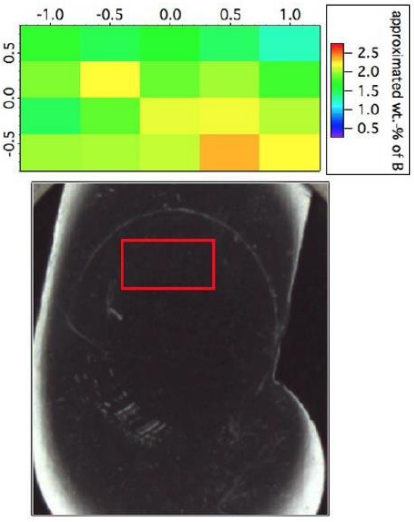

Fig. 2 The XRF mapping of B on the welded steel sample. The x and y scale shown on the map is in mm. The weight ratio of B to (B+Fe+Cr) is approximately 0.0186.

2.2. In-situ Observation During Thermal Annealing by LEEM and PEEM

LEEM and PEEM were conducted at Beamline 3.2Ub: PEEM at the Synchrotron Light Research Institute. The end-station is Elmitec SPLEEM-III equipped with an imaging electron energy analyzer. The base pressure in the analysis chamber is in the low 10^{-10} mbar. Before the experiment, the Fe alloy sample was clean by Ar^+ sputtering at the energy of 1 kV for 1 hour. After being introduced into the analysis chamber, they were heated radiatively from RT to ~500 °C to degas for several hours. During the h-BN growth, the sample was further heated by electron-beam bombardment to the backside. The temperature was measured by a type-C thermocouple attached to the base metal ring placed under the sample. For LEEM, LEED and EELS, the LaB6 cathode source is used (the beam energy spread is around 1 eV). For PEEM, an undulator produces a linear-horizontal photon with the glancing angle of ~17° to the surface of the sample (s-polarization). The imaging electron energy analyzer has an energy resolution of around 0.3 eV in dispersive XPS measurement, with a selected-area aperture to select the microscopic area (~10 um). Imaging NEXAFS was performed by recording a series of PEEM images with the change in photon energy across the absorption edge of selected elements. Image analyses to determine island sizes and densities were performed using Image Processing package in Igor Pro software.

First, for each LEEM image the intensity background was corrected. Then a threshold image was created under a defined intensity level (same for all images). A median convolution filter (5 by 5 pixels) was used three times to remove noise in the threshold image. Then *ImageParticleAnalysis* function in Igor Pro was used to find statistics of h-BN sizes and island density for each image. Note that 20% error bars were applied in the average island sizes to represent possible errors for h-BN islands that appeared at the edge of LEEM's micro-channel plate screen and also ones that were too small or too dark. 10% error bars were applied for the island density because the island counts were less susceptible to errors that were caused by the same reasons.

3. Results and Discussions

3.1. In-situ Growth of h-BN

After being cleaned by an Ar^+ sputter gun and then degassed at 300 °C for more than 10 hours, the sample was introduced to the analysis chamber of LEEM. As the largest field of view of our LEEM system is around 75 μm, it was not possible to observe nucleation of h-BN simultaneously on Metal A, the interface, and Metal B areas during the annealing. For in-situ observation during the temperature annealing cycles, we chose to image the region on Metal A near the interface where the effects from the diffusion of B and N atoms could be monitored. When the sample was heated up to around 600 °C, surface precipitates started to appear under LEEM as shown by the left-most image in Fig. 3a. While the grain contrast in LEEM which is normally observed for polycrystalline samples was not yet seen (because the Ar^+ cleaning resulted in the disordering of the crystal structure on the surface), surface precipitates which nucleated as small dark domains tended to reside along straight lines which resembled grain boundaries of the alloys. This contrast between the surface precipitates and the alloy substrate in LEEM was due to the difference in work functions [22]. The precipitates became larger and coalesced into each other to form large dark domains. After the temperature was further increased to around 650 °C, the dark domains started to disappear, suggesting that the atoms that formed the first-stage precipitation dissolved back into the bulk.

The precipitates completely disappeared as the sample temperature was increased above approximately 700 °C

(the exact temperature can vary by ± 30 °C because the thermocouple did not directly touch the surface). After that, the sample temperature was reduced, resulting in a formation of triangular-shaped dark h-BN phases in LEEM in Fig. 3b. In the second precipitation, the nucleation density was much lower, and the shape and the orientation were better defined. Within the same grain of the polycrystalline alloys, many of the h-BN precipitates share either the same orientation or one with 30° rotation (Fig. 4). The chemical analysis of this dark triangular phase was performed to confirm the species as h-BN (the details are provided in the next section). Note that although the chemical composition of the first-stage precipitates was not identified, the contrast between the second triangular h-BN and the metal alloy appeared similar to the first-stage precipitation which suggests that they are the same species.

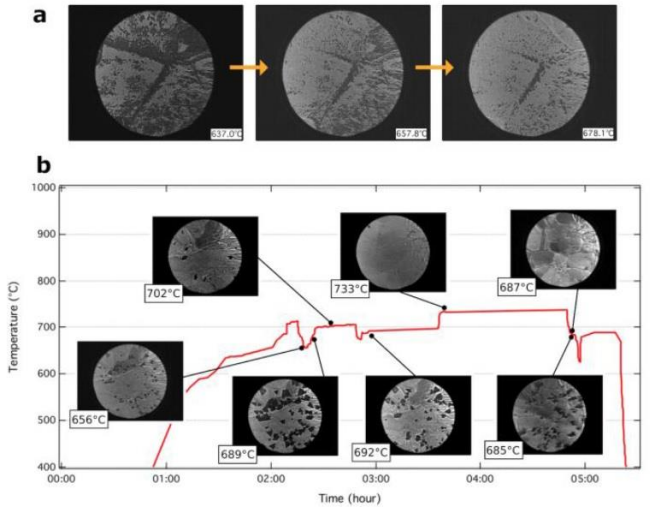

Fig. 3 (a) Initial stage of formation. (b) Temperature profile with snapshots of LEEM images (75 μm field of view) in the same area during the formation of h-BN at the weld interface by thermal annealing.

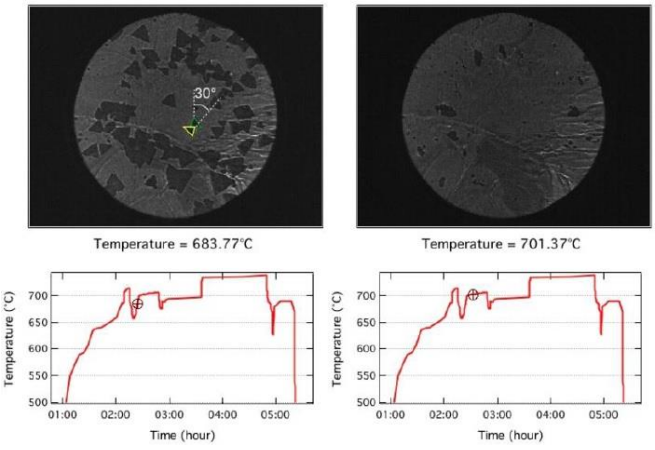

Fig. 4 A snapshot of the in-situ LEEM observation during h-BN growth (75 μm field of view). The video could be seen from https://youtu.be/pnEAm1KjWKs. Most of the triangular h-BN islands in the same Fe grains either share the same orientation or are 30° rotated from each other.

Reversibility of h-BN formation was evident when the temperature was raised one more time up to above 700 °C and the dark h-BN phases disappeared again in a similar fashion as when the first-stage precipitations had disappeared before. We experimented with temperature cycling below and above 700 °C (a video provided in https://youtu.be/pnEAm1KjWKs) and confirmed that the formation of the triangular h-BN was reversible, i.e., h-BN disappeared when the temperature was raised above 700 °C, and re-appeared when the temperature was lowered below 700 °C. The nucleation locations of h-BN islands for each cycle were somewhat unchanged when the range of the temperature swing was small and was more random when the range was wider or when the sample was held above 700 °C for a longer period. This might be the evidence for the diffusion of B and N in one type of crystal structure at high temperature and segregation from the other type. The change in nucleation sites was probably due to the microstructural changes in the Fe alloy during the BCC-FCC phase transition which happened at around the same temperature (so-called A_1 line in Fe-C phase diagram). In the final step, the sample temperature was held at 690 °C for 30 minutes, and then the heater was immediately shut down to let the sample cool at the rate of around 100 °C per minute. During the quench, LEEM showed that the size of h-BN remained constant (at least within the field of view being observed).

3.2. Characterization of Triangular h-BN Islands

After the sample was cooled down to room temperature, characterizations of h-BN islands on the surface were performed using LEEM and low-energy electron diffraction (LEED), together with x-ray photoelectron spectroscopy (XPS) and near-edge x-ray absorption fine structure (NEXAFS) using synchrotron soft x-ray as shown by Fig. 5a-f. A stitched LEEM image of the surface after the final formation of h-BN along ~1400 μm crossing the interface region between Metal A and B is shown in Fig. 5a. The density and the average size of the triangular h-BN islands varied greatly across the joined interface - there were very few h-BN islands on Metal B and many on Metal A (on the left- and right-hand sides of Fig. 5a, respectively). The transition region where low density of h-BN islands formed but the average size of the islands was significantly larger spanned around the 200 μm into the weld zone in Metal B. High-magnification LEEM images of one of the large h-BN islands at the start voltage of 0.22 eV and 19.80 eV are shown in Fig. 5b and c. For LEEM image at higher electron incidence energy (19.80 eV in Fig. 5c), there is a strong contrast between the h-BN flake and the bare metal alloy surface, while at lower electron incidence energy (0.22 eV in Fig. 5b) the contrast between the tip and the center area of the h-BN island shows up.

Selective-area XPS and NEXAFS were used to determine the composition and the chemical states of the large h-BN island. XPS with 630 eV photon energy (Fig.

5g) showed a large amount of N on h-BN in comparison to on the bare alloy substrate. The difference in B 1s peaks between h-BN island and Fe alloy substrate could be seen more clearly in Fig. 5h for XP spectrum with lower excitation energy at 405 eV where the surface sensitivity was higher due to smaller escape depth of the photoelectrons. Imaging N K-edge and B K-edge NEXAFS scans (Fig. 5d and e) of the h-BN island and the surrounding bare alloy substrate showed not only a clear difference in the amount of B and N, but also the fine-structure features which are consistent with NEXAFS of h-BN reported in literature elsewhere [23, 24]. Note that in our NEXAFS measurements, the polarization of the photon beam produced from the planar undulator was fixed to the linear-horizontal orientation. With the sample facing down in our PEEM setup, the incidence x-ray was S-polarized. NEXAFS is angular dependent and, in theory, may not show molecular orbitals with polarization perpendicular to the surface. The fact that both π^* and σ^* peaks were both present in B K-edge, and N K-edge spectra in the measurements could mean that the two-dimensional structure of h-BN was not aligned with the sample surface, or that the surface of the sample inside PEEM chamber itself was not perfectly aligned to the polarization of the x-ray beam. NEXAFS for the h-BN in this work showed no sign of hybridization as previously reported by h-BN grown on a different substrate (Ni foil) [23] and h-BN grown by CVD [24]. This could be due to the weaker interaction between h-BN and the Fe alloy compared to Ni. Sharp hexagonal pattern (Fig. 5f) from micro-LEED with a 5-μm diameter selected area aperture confirmed the well-ordered atomic structure of h-BN. The LEED pattern also showed two different rotating domains (off from each other by around 15°) on different parts of the observed h-BN island (not shown). Also seen from Fig. 5b were the tips of the h-BN island similar to that reported by Xu et al [18] which suggested higher concentration of atomic S impurity that is prevalent in most Fe steels. Work-function mapping in Fig. 6 showed that the tips with S impurity had the work function around 0.2 eV lower than the center area of the h-BN island. Higher magnification LEEM image (Fig. 7) also showed unique structure of the tips with stripe patterns with about 60° different orientation between each other.

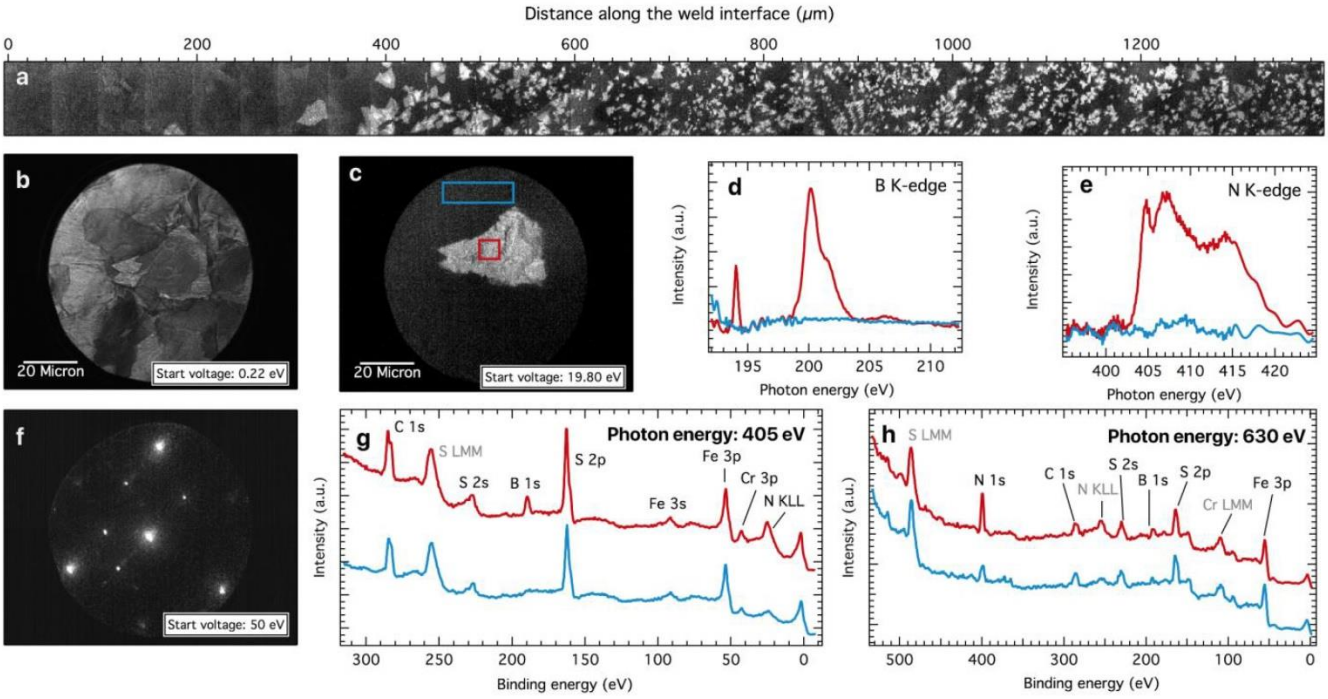

Fig. 5 (a) Stitched LEEM image (start voltage = 5.21 eV) of the surface after forming the triangular phase showing an area across the welded interface. The right-hand side is the base metal (Metal A) and the left-hand side is the weld metal (Metal B). h-BN is small with high nucleation density on the base metal side, large with low nucleation density at the welding interface, and not present at the weld metal side. (b, c) LEEM image of a large h-BN island at the start voltages of 0.22 and 19.80 eV, respectively. (d, e) NEXAFS spectra in the B K-edge and N K-edge regions, respectively. The spectra were acquired from the red and blue boxes in (c). (f) LEED at 50 eV electron incidence energy. (g) Selected-area survey XP spectra using the photon energy of 630 eV for h-BN (red) and substrate (blue). (h) Selected-area survey XP spectra using the photon energy of 405 eV for h-BN (red) and substrate (blue).

The variation of reflected-electron intensity as a function of the incidence energy in LEEM (LEEM-IV) is a convenient tool for determining thicknesses of two-dimensional materials including few-layer h-BN [25, 26]. As shown in Fig. 8, the IV curves with fine features originating from the electron interactions with discreet electronic states of two-dimensional h-BN could be observed in the incidence energy range between 0 and 20

eV. Similar to graphene where the number of layers shows up as the oscillation in the IV curves [25] for h-BN the thickness difference appears as the oscillation in the 0 to 5 eV region [26]. The IV curve could also be used to identify bare alloy surfaces without h-BN (no peaks at 7 eV and 13 eV) [27], allowing for the determination of h-BN coverage. Figure 8a shows the IV-curve of the large h-BN island at the interface region (the same island as the one in Fig. 5b and c). The oscillation suggested the thickness of 3 atomic layers and no difference between the tip with S impurities and the center of the h-BN island. In comparison, the same measurement from the area inside the Metal A (Fig. 8b) showed different shapes of IV-curves suggesting the thickness varied between 3-4 layers. The ~6 eV bandgap of the large h-BN flake in Fig. 5c was confirmed by micro-electron-energy loss spectroscopy (EELS) (Fig. 9).

3.3. Discussion

Precipitations of impurities in metal alloys have been studied extensively by metallurgical engineers for many decades using conventional material analysis tools such as x-ray diffraction and transmission electron microscopy. Most works have focused on precipitations inside the bulk, mainly happening at the grain boundaries or inside the grains of metals, as the phenomena strongly affect bulk mechanical properties when they are used as engineering materials. Although surface precipitations may seem somewhat less important in that regard, there have been a few studies which aim specifically for surface applications, for examples, to create BN coating on steels to make the surface more inert to chemical reaction (e.g., oxidation), and to suppress degassing inside vacuum chambers [28, 29]. Early observations of surface precipitations of BN by Stulen and Bastasz in 1979 [30] by electron spectroscopy and microscopy occurred long before the realization of the quantum size effects in two-dimensional materials [31].

Later on, Minami et al [32] tested the effects of the bulk concentrations of B and N in steels and found that the concentration of N needed to be higher than around 0.1 wt% for BN to form on the surface. For B, however, too high B concentration resulted in BN forming in bulk instead. In their theoretical model, it was assumed that the temperature required for the reaction to form BN is 700 °C. In contrast with our LEEM in-situ observation, it could be seen from repeating cycles of heating and cooling around the same temperature that the formation of h-BN did not happen during the temperature rise, but actually happened during the cool down period, a process which reduces the solubility of impurity atoms and drives them from bulk to surface. This means the formation of h-BN during the annealing was limited by diffusion of atoms rather than thermal energy. The temperature higher than 700 °C instead dissociated h-BN and drove the atoms down to the bulk. This argument is supported by the plot of h-BN island size and temperature as functions of time from the in-situ observation in Fig. 10a.

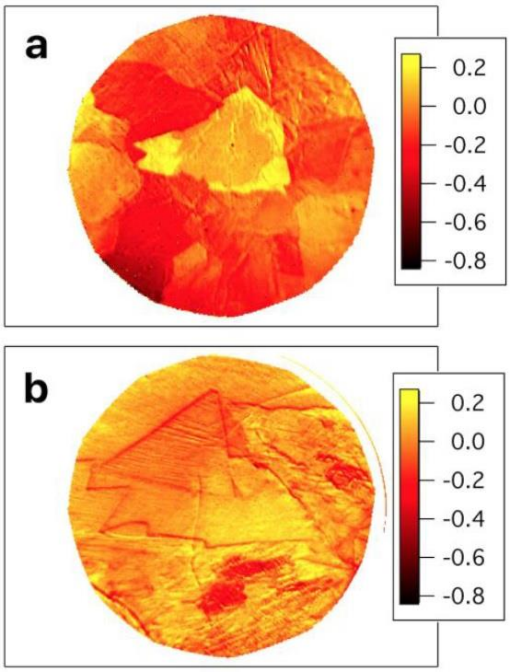

Fig. 6 Relative work function maps of (a) a large h-BN island on the interface region and (b) many h-BN islands which formed on the Metal B side.

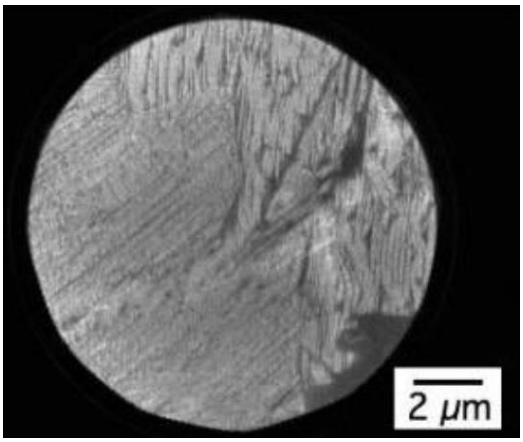

Fig. 7 High resolution LEEM image of the tip of h-BN island showing a striped structure.

Some aspects related to h-BN formation mechanism may be deduced from three main observations in our LEEM experiments: (1) the appearance and disappearance of h-BN due to Fe phase transition, (2) the diffusion from bulk to the surface mainly along the grain boundaries, and (3) the laterally nonhomogeneous growth of h-BN islands due to the diffusion across the weld interface between two different metal alloys. Phase transition of Fe-based alloys at around 700 °C which causes the grain structure to change plays a very important role in driving the impurity atoms to and from inside the bulk. Because the size of interstitial sites in FCC (the structure of Fe at higher temperature) is larger than those of BCC (the structure of Fe at lower temperature), interstitial B and N atoms are driven out from inside the grains to the grain boundary first, and then driven to the surface by thermal energy. Figure 10b shows a histogram of the nearest distance from each h-BN nucleation site to the grain boundary of the

steel in the observed field of view of LEEM during the last temperature swing cycle (the bottom right inset in Fig. 3b). Large populations of h-BN which nucleated within 3 μm from grain boundaries suggests that the diffusions of B and N atoms occur along the grain boundaries prior to h-BN formations (the average grain size is around 10 μm for near-surface microcrystalline grains on the Metal A side). The observation in this work is different from that in Xu et al [17] which do not show preference in precipitation near grain boundaries. This is probably due to the temperature difference that may strongly affect the mobility of B and N atoms on the surface.

Figure 10c demonstrates the inhomogeneity of the nucleation density and the average island size of h-BN in the vicinity of the weld interface. Nucleation was relatively dense in Metal A (HAZ) and became sparser moving toward Metal B (weld zone). The island size was the largest at the interface region (at the position of 400 μm in the plot) and became smaller and more uniform around 100 μm away toward Metal A. A combination of factors that possibly affected the inhomogeneous nucleation and growth rates includes – (1) the smaller average grain size in Metal A, (2) the difference in the atomic percentages of B, N and S impurities between the two metals and (3) the small difference in the phase transition temperature which resulted from the different bulk chemical compositions due to the dilution between base metal (A) and filler metal (B) from welding process.

The LEEM observation suggested that there should be more B in Metal A although according to the ASME standard, B and N contents in the material used in this study (2.25Cr-1Mo and ER90S-B9) are not specified in their composition tables. A very small amount of B but enough to segregate on the surface to form h-BN have been reported before [33]. Also, it was highly likely that, similar to S, N was already presented inside most steels, and both Metal A and B should contain enough supplies of the atoms. Apart from the amounts of impurities, the microstructure should be another important factor that affected the diffusion of the B and N atoms, and the difference in the sizes and shapes of grains in the two metals must be taken into account. The I-V curve in LEEM [34] helped to identify the number of layers of h-BN [26, 27] to compare the thickness of h-BN in different areas. It was found form I-V LEEM that most h-BN in the middle of the weld interface was tri-layer, and in the Metal A side, there exist multiple h-BN domains with varying thicknesses between 3-4 atomic layers. This finding suggested that there were more localized channels for B and N atoms to diffuse from bulk to surface possibly via denser grain boundaries/smaller grain size compared to weld zone and contribute to the thickness increase of individual multi-layer h-BN and that diffusion from bulk to surface is fast in comparison to the lateral diffusion of B and N atoms. While previous reports have mentioned the difficulties in controlling the thickness of the h-BN in precipitation method, with some control over the diffusion of atoms by using metallurgical processes to alter the grain sizes, orientations and crystallographic structures, it should be possible to engineer the growth of h-BN toward the desired sizes and thicknesses, for examples, by changing alloying compositions and heat and mechanical treatments of the metals.

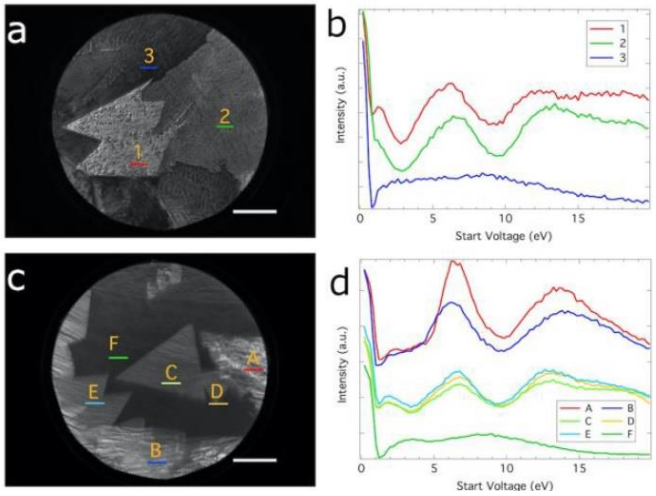

Fig. 8. IV characteristic of h-BN. (a), (b) single h-BN flake formed at the interface. (c), (d) multiple h-BN flakes on the base metal (Metal A) side. The field of view in (a) and (c) is 25 μm.

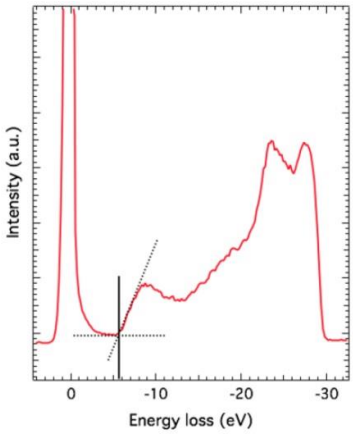

Fig. 9. Micro reflective EELS spectra measured on h-BN in Figure 2c showing the bandgap of h-BN of around 6 eV.

The work function difference between the S-rich corners and the middle point of h-BN flake are shown in Fig. 6. According to studies from Yoshihara et al, and later from Minami et al, S impurity limits the growth of surface BN [29, 32]. More recent characterization of h-BN created by surface precipitation from Xu et al [17] gives an insight into the growth mechanism in which the intermediate layer of the two-dimensional surface structure containing B, N and S atoms formed before h-BN grows on top. They also report the cap domains at the corners of triangular h-BN flakes which contain more S in comparison to the middle part. This is due to the driving force to form highly thermodynamically stable h-BN which pushes S atoms away possibly to the edge and

corner of the two-dimensional structure. While it was not yet clear how the S-rich caps affected the growth in this work, NEXAFS and LEEM-IV measurements from the cap and the middle area of h-BN did not show the difference in the chemistry and electronic structure (although we observed the lamella pattern [35] in the cap domain sunder high-magnification LEEM as shown in Fig. 7). This point will be further investigated using real-time observation of LEEM and PEEM in future work.

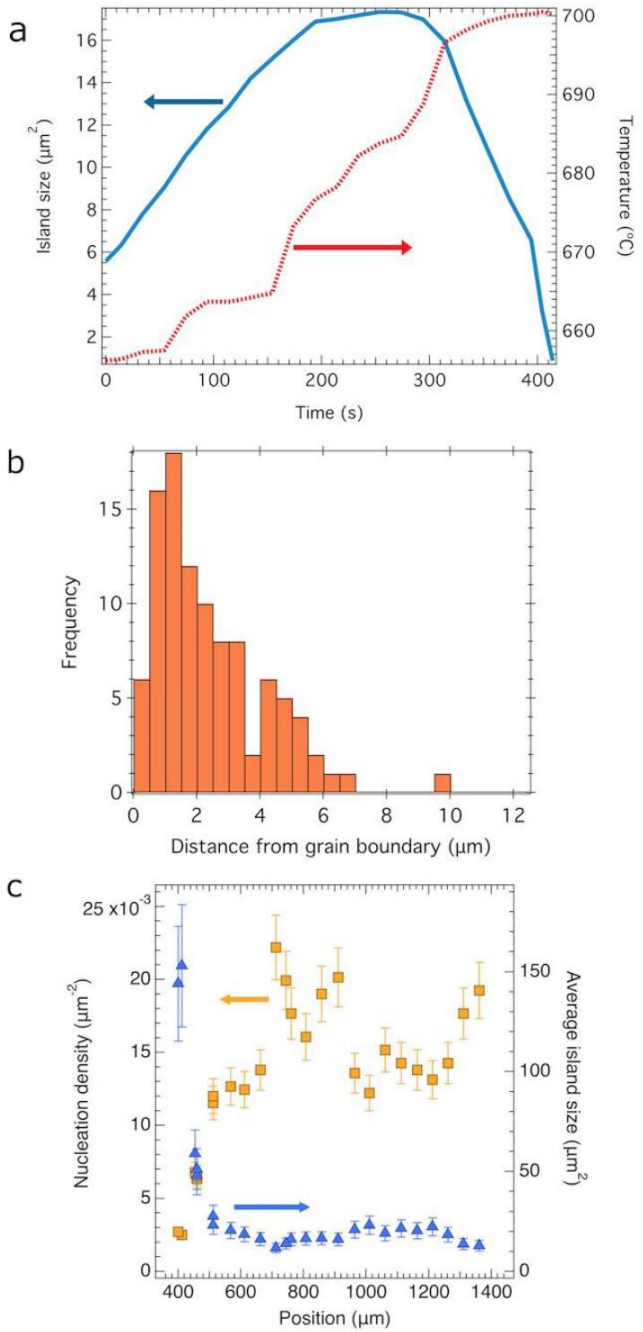

Fig. 10. (a) average island size and temperature of the sample as a function of time during the temperature ramp. (b) a histogram showing the nearest distance of the nucleation points of h-BN islands from the grain boundaries. (c) nucleation density of h-BN and average island size as a function of the position across the weld interface.

4. Conclusions

Reversible formation of h-BN has directly been observed on the surface of joined dissimilar steels suggesting the significant role of the structures and impurities in the metal substrates to the behaviors of the h-BN growth. When the temperature of the sample was raised toward the BCC-FCC transition temperature, B and N diffused inside the metals along the grain boundary. Once the temperature went above the BCC-FCC transition, and then subsequently came down for Fe to change back to BCC, the phase transition drove B and N to the surface to react and form h-BN. LEEM observation on many cycles of temperature swing confirmed the reversibility of the reaction (when the temperature is raised higher temperature h-BN dissociated and the B and N atoms diffused back into the bulk metal again). The real-time imaging during the annealing experiments suggests that the formation of h-BN was diffusion-limited rather than reaction-limited. After the sample had been quenched down to room temperature, the post-annealing characterization by LEEM and PEEM were performed to confirm that the resulting few-layer h-BN had similar chemistry and atomic structure of the h-BN synthesized by other methods. By understanding the combinations of effects from crystal and microscopic (grain) structures, impurities, and especially the phase transition, the diffusion of B and N atoms can be better controlled so that the coverage and thickness of h-BN that forms on the surface can be made suitable for applications such as protecting the surface of steels under harsh conditions. Proposed future works may include study of the h-BN growth on different types of steels which contains different mixtures of BCC-FCC phases which should strongly affect how h-BN grows according to our finding in this work. Further experiments will focus on how much h-BN can perform to protect the surface in various simulated environments.

Acknowledgement

Authors would like to thank Natthaphong Konkhunthot, Prapaporn Silawong, and Nattapol Pintitraratibodee for assisting in LEEM and PEEM experiments. Also, high appreciation would be given to Sudarat Khetsoongnoen for preparing and providing experimental specimens.

References

[1] X. Li *et al.*, "Graphene and related two-dimensional materials: Structure-property relationships for electronics and optoelectronics," *Appl. Phys. Rev.*, vol. 4, no. 2, p. 021306, 2017.

[2] R. Kumar, S. Sahoo, E. Joanni, R. K. Singh, R. M. Yadav, R. K. Verma, D. P. Singh, W. K. Tan, A. Pérez del Pino, S. A. Moshkalev, and A. Matsuda, "A review on synthesis of graphene, h-BN and MoS2 for energy

storage applications: Recent progress and perspectives," *Nano Res.*, vol. 12, pp. 2655–2694, 2019.
[3] K. Zhang, Y. Feng, F. Wang, Z. Yang, and J. Wang, "Two dimensional hexagonal boron nitride (2D-hBN): synthesis, properties and applications Materials Chemistry C," *J. Mater. Chem. C*, vol. 5, pp. 11992–12022, 2017.
[4] L. Wang *et al.*, "Water-assisted growth of large-sized single crystal hexagonal boron nitride grains," *Mater. Chem. Front.*, vol. 1, no. 9, pp. 1836–1840, 2017.
[5] H. Cun *et al.*, "Centimeter-sized single-orientation monolayer hexagonal boron nitride with or without nanovoids," *Nano Lett.*, vol. 18, no. 2, pp. 1205–1212, 2018.
[6] S. Pyo, J. Choi, and J. Kim, "Improved photo- and chemical-responses of graphene via porphyrin-functionalization for flexible, transparent, and sensitive sensors," *Nanotechnology*, vol. 30, no. 21, p. 215501, 2019.
[7] L. Lipani *et al.*, "Non-invasive, transdermal, path-selective and specific glucose monitoring via a graphene-based platform," *Nat. Nanotechnol.*, vol. 13, no. 6, pp. 504–511, 2018.
[8] C. G. Núñez, W. T. Navaraj, E. O. Polat, and R. Dahiya, "Energy-autonomous, flexible, and transparent tactile skin," *Adv. Funct. Mater.*, vol. 27, no. 18, p. 1606287, 2017.
[9] K. Watanabe, T. Taniguchi, and H. Kanda, "Direct-bandgap properties and evidence for ultraviolet lasing of hexagonal boron nitride single crystal," *Nat. Mater.*, vol. 3, no. 6, pp. 404–409, 2004.
[10] F. Mahvash, S. Eissa, T. Bordjiba, A. C. Tavares, T. Szkopek, and M. Siaj, "Corrosion resistance of monolayer hexagonal boron nitride on copper," *Sci. Rep.*, vol. 7, p. 42139, 2017.
[11] H. Wu *et al.*, "Dynamic nanoscale imaging of enriched CO adlayer on Pt(111) confined under h-BN monolayer in ambient pressure atmospheres," *Nano Res.*, vol. 12, no. 1, pp. 85–90, 2019.
[12] R. Zhang, J. Zhao, J. Pu, and Z. Lu, "First-principles investigation on the tribological properties of h-BN bilayer under variable load," *Tribol. Lett.*, vol. 66, no. 4, p. 124, 2018.
[13] H. Wang, Y. Zhao, Y. Xie, X. Ma, and X. Zhang, "Recent progress in synthesis of two-dimensional hexagonal boron nitride," *J. Semicond.*, vol. 38, no. 3, p. 031003, 2017.
[14] W. Auwärter, "Hexagonal boron nitride monolayers on metal supports: Versatile templates for atoms, molecules and nanostructures," *Surf. Sci. Rep.*, vol. 74, no. 1, pp. 1–95, 2019.
[15] S. Masubuchi *et al.*, "Deep-learning-based image segmentation integrated with optical microscopy for automatically searching for two-dimensional materials," *npj 2D Mater. Appl.*, pp. 4–6, 2019.
[16] S. Masubuchi *et al.*, "Autonomous robotic searching and assembly of two-dimensional crystals to build van der Waals superlattices," *Nat. Commun.*, vol. 9, no. 1, pp. 4–6, 2018.
[17] M. Xu, D. Fujita, H. Chen, and N. Hanagata, "Formation of monolayer and few-layer hexagonal boron nitride nanosheets via surface segregation," *Nanoscale*, vol. 3, no. 7, pp. 2854–2858, 2011.
[18] S. Suzuki, R. M. Pallares, and H. Hibino, "Growth of atomically thin hexagonal boron nitride films by diffusion through a metal film and precipitation," *J. Phys. D. Appl. Phys.*, vol. 45, no. 38, p. 385304, 2012.
[19] C. Zhang, L. Fu, S. Zhao, Y. Zhou, H. Peng, and Z. Liu, "Controllable co-segregation synthesis of wafer-scale hexagonal boron nitride thin films," *Adv. Mater.*, vol. 26, no. 11, pp. 1776–1781, 2014.
[20] I. Phung-on, S. Khetsoongnoen, J. Srithorn, C. Euaruksakul, and P. Photongkam, "In - situ observation of martensite decomposition in HAZ of Cr - Mo steel weldment," *Eng. J.*, vol. 23, no. 5, pp. 59–70, 2019.
[21] S. Khetsoongnoen, J. Srithorn, I. Phung, C. Euaruksakul, P. Photongkam, and T. Wongpinij, "In - situ observation of carbide precipitation in dissimilar joining of Cr - Mo steel," *Suranaree J. Sci. Technol.*, vol. 26, no. 3, pp. 284–292, 2019.
[22] P. L. Levesque, H. Marchetto, T. Schmidt, F. C. Maier, H. J. Freund, and E. Umbach, "Correlation between substrate morphology and the initial stages of epitaxial organic growth: PTCDA/Ag(111)," *J. Phys. Chem. C*, vol. 120, no. 34, pp. 19271–19279, 2016.
[23] S. Suzuki *et al.*, "Quasi-free-standing monolayer hexagonal boron nitride on Ni," *Mater. Res. Express*, vol. 6, no. 1, p. 016304, 2019.
[24] A. B. Preobrajenski, A. S. Vinogradov, and N. Mårtensson, "Ni 3d-BN π hybridization at the h-BN/Ni(111) interface observed with core-level spectroscopies," *Phys. Rev. B - Condens. Matter Mater. Phys.*, vol. 70, no. 16, p. 165404, 2004.
[25] H. Hibino, H. Kageshima, F. Maeda, M. Nagase, Y. Kobayashi, and H. Yamaguchi, "Microscopic thickness determination of thin graphite films formed on SiC from quantized oscillation in reflectivity of low-energy electrons," *Phys. Rev. B - Condens. Matter Mater. Phys.*, vol. 77, no. 7, p. 075413, 2008.
[26] J. Jobst, J. Kautz, D. Geelen, R. M. Tromp, and S. J. Van Der Molen, "Nanoscale measurements of unoccupied band dispersion in few-layer graphene," *Nat. Commun.*, vol. 6, pp. 1–6, 2015.
[27] C. M. Orofeo, S. Suzuki, H. Kageshima, and H. Hibino, "Growth and low-energy electron microscopy characterization of monolayer hexagonal boron nitride on epitaxial cobalt," *Nano Res.*, vol. 6, no. 5, pp. 335–347, 2013.
[28] D. Fujita and T. Homma, "A new model of surface precipitation of boron nitride on an austenitic stainless steel and its outgassing nature," *Thin Solid Films*, vol. 181, no. 1–2, pp. 267–276, Dec. 1989.
[29] K. Yoshihara, M. Tosa, and K. Nii, "Surface precipitation of boron nitride on the surface of type 304 stainless steels doped with nitrogen, boron, and

cerium," *J. Vac. Sci. Technol. A Vacuum, Surfaces, Film.*, vol. 3, no. 4, pp. 1804–1808, 1985.
[30] R. H. Stulen and R. Bastasz, "Surface segregation of boron in nitrogen-strengthened stainless steel," *J. Vac. Sci. Technol.*, vol. 16, no. 3, pp. 940–945, 1979.
[31] K. S. Novoselov *et al.*, "Two-dimensional gas of massless Dirac fermions in graphene," *Nature*, vol. 438, no. 7065, pp. 197–200, 2005.
[32] Y. Minami, A. Tohyama, and T. Yamada, "Effect of some elements and temperature on the surface segregation of boron nitride," *J. Vac. Sci. Technol. A Vacuum, Surfaces, Film.*, vol. 7, no. 3, pp. 1585–1588, 1989.
[33] C. A. Long and H. J. Grabke, "The formation of boron nitride on Fe37Ni alloy," *Appl. Surf. Sci.*, vol. 59, no. 3–4, pp. 207–217, 1992.
[34] J. I. Flege and E. E. Krasovskii, "Intensity-voltage low-energy electron microscopy for functional materials characterization," *Phys. Status Solidi - Rapid Res. Lett.*, vol. 8, no. 6, pp. 463–477, 2014.
[35] Y. S. Kim, K. S. Lee, J. Lee, M. Tosa, A. Kasahara, and K. Yosihara, "Surface segregation of hexagonal boron nitride and its surface properties," *J. Vac. Sci. Technol. A Vacuum, Surfaces, Film.*, vol. 19, no. 3, pp. 1013–1017, 2002.

Chanan Euaruksakul was born in Bangkok, Thailand in 1979. He received the Bachelor Degree in electrical engineering from Chulalongkorn University, Bangkok and Master Degree in electrical and computer engineering in 2004, and PhD in elecrical engineering in 2009 from University of Wisconsin – Madison.

From 2009 to 2013, he was a Beamline Scientist for Beamline 3.2Ub:PEEM of the Synchrotron Light Research Institute (Public Organization). His research focuses on surface science and ultra-thin films with emphasis on using low-energy electron microscopy and photoemission electron microscopy techniques.

Isaratat Phung-on was born in Lopburi, Thailand in 1978. He got a Bachelor Degree in Production Engineering from KMUTT, Bangkok, Thailand in 1999. After, his interests moved to welding technology and received the M.S. and Ph. D. in Weldgin Engineer from The Ohio State University, USA in 2003 and 2007. Starting form 2007, he is working as a research scientist at Maintenance Technology Center, ISTRS, KMUTT, Thailand. His research fields are about welding metallurgy, failure analysis, as well as product development related to welding, non-destructive testing, and materials.

Jongkol Srithorn was born in Bangkok, Thailand in 1979. He received the Bachelor Degree in electrical engineering from Chulalongkorn University, Bangkok and Master Degree in electrical and computer engineering in 2004, and PhD in elecrical engineering in 2009 from University of Wisconsin – Madison.

From 2009 to 2013, he was a Beamline Scientist for Beamline 3.2Ub:PEEM of the Synchrotron Light Research Institute (Public Organization). His research focuses on surface science and ultra-thin films with emphasis on using low-energy electron microscopy and photoemission electron microscopy techniques.

Thipusa Wongpinij was born in Nakhonratchasima, Thailand in 1986. She received the Bachelor Degree and Master Degree in metallurgical engineering in 2012 from Suranaree University of Technology, Nakhonratchasima.

From 2014 to Present, She was a Research Assistant at the beamline, BL3.2Ub: PEEM of Synchrotron Light Research Institute (Public Organization), Thailand. Her research focuses on surface science, corrosion behaviors of metals, analysis of DLC and thin films by Synchrotron-based analytical techniques: near-edge X-ray absorption fine structure (NEXAFS) spectroscopy and X-ray photoemission electron microscopy (XPS) and thin films using low energy electron microscopy and photoemission electron microscopy techniques.

Pat Photongkam was born in Greenwich Village, New York, NY, USA in 1977. He received the B.S. and M.S. degrees in aerospace engineering from the University of Virginia, Charlottesville, in 2001 and the Ph.D. degree in mechanical engineering from Drexel University, Philadelphia, PA, in 2008.

From 2001 to 2004, she was a Research Assistant with the Princeton Plasma Physics Laboratory. Since 2009, she has been an Assistant Professor with the Mechanical Engineering Department, Texas A&M University, College Station. She is the author of three books, more than 150 articles, and more than 70 inventions. Her research interests include high-pressure and high-density nonthermal plasma discharge processes and applications, microscale plasma discharges, discharges in liquids, spectroscopic diagnostics, plasma propulsion, and innovation plasma applications. She is an Associate Editor of the journal Earth, Moon, Planets, and holds two patents.

Krongthong Kamonsuangkasem was born in Bangkok, Thailand in 1985. She recieved the Bachelor Degree in Industrial Chemistry from King Mongkut's Institute of Technology Ladkrabang in 2007 and the Master degree in Chemical Engineering from King Mongkut's University of Technology Thonburi in 2010, and the Ph.D. degree in Energy Technology from the Joint Graduated School of Energy and Environment, King Mongkut's University of Technology Thonburi in 2017.

From 2017 to 2018, she was a postdoctoral researcher with Beamline 1.1W, Synchrotron Light Research (Public Organization), Thailand. Since 2018, she has been a beamline scientist for Applied Research for Industry as well as for Beamline 1.1W, Synchrotron Light Research (Public Organization), Thailand. Her research interests include heterogeneous catalysts, hydrogen production from biomass, catalyst characterization and fuel cell application.

Neeranut Aimkogsung was born in Nakhon Ratchasima, Thailand in 1988. She recieved the Bachelor Degree of Engineering in Ceramic Engineering from Suranaree University of Technology, Nakhon Ratchasima, Thailand in 2010.

From 2009 to 2010, she was a co-op student with COTTO (Thaliand) Co., Ltd. Her research focuses on the product development in terms of process and raw materials. Since 2019, she has been a laboratory scientist at Synchrotron Light Research Institute (Public Organization), Thailand. Her research interests include ferroelectrics and piezoelectric materials as well as analysis of structural clay products by using X-ray based techniques: X-ray diffraction, X-ray fluorescence and X-ray absorption spectroscopy.